

# The effects of the small-scale DM power on the cosmological neutral hydrogen (HI) distribution at high redshifts

Abir Sarkar,<sup>1,2</sup> Rajesh Mondal,<sup>3,4</sup> Subinoy Das,<sup>5</sup> Shiv.K.Sethi,<sup>1</sup>  
Somnath Bharadwaj,<sup>3,4</sup> David J. E. Marsh<sup>6</sup>

<sup>1</sup>Raman Research Institute,  
Bangalore, India

<sup>2</sup>Indian Institute of Science,  
Bangalore, India

<sup>3</sup>Department of Physics, Indian Institute of Technology Kharagpur,  
Kharagpur - 721302, India

<sup>4</sup>Centre for Theoretical Studies, Indian Institute of Technology Kharagpur,  
Kharagpur - 721302, India

<sup>5</sup>Indian Institute of Astrophysics,  
Bangalore, India

<sup>6</sup>Department of Physics, King's College London,  
Strand, London, WC2R 2LS, United Kingdom

E-mail: [abir@rri.res.in](mailto:abir@rri.res.in), [rm@phy.iitkgp.ernet.in](mailto:rm@phy.iitkgp.ernet.in)

**Abstract.** The particle nature of dark matter remains a mystery. In this paper, we consider two dark matter models—Late Forming Dark Matter (LFDM) and Ultra-Light Axion (ULA) models—where the matter power spectra show novel effects on small scales. The high redshift universe offers a powerful probe of their parameters. In particular, we study two cosmological observables: the neutral hydrogen (HI) redshifted 21-cm signal from the epoch of reionization, and the evolution of the collapsed fraction of HI in the redshift range  $2 < z < 5$ . We model the theoretical predictions of the models using CDM-like N-body simulations with modified initial conditions, and generate reionization fields using an excursion-set model. The N-body approximation is valid on the length and halo mass scales studied. We show that LFDM and ULA models predict an increase in the HI power spectrum from the epoch of reionization by a factor between 2–10 for a range of scales  $0.1 < k < 4 \text{ Mpc}^{-1}$ . Assuming a fiducial model where a neutral hydrogen fraction  $\bar{x}_{HI} = 0.5$  must be achieved by  $z = 8$ , the reionization process allows us to put approximate bounds on the redshift of dark matter formation  $z_f > 4 \times 10^5$  (for LFDM) and the axion mass  $m_a > 2.6 \times 10^{-23} \text{ eV}$  (for ULA). The comparison of the collapsed mass fraction inferred from damped Lyman- $\alpha$  observations to the theoretical predictions of our models lead to the weaker bounds:  $z_f > 2 \times 10^5$  and  $m_a > 10^{-23} \text{ eV}$ . These bounds are consistent with other constraints in the literature using different observables and, in the case of ULAs, are also consistent with a solution to the cusp-core problem of CDM.

**Keywords:** cosmology: theory - Epoch of Reionization - large-scale structure - methods: numerical

**ArXiv ePrint:** [1511.00000](https://arxiv.org/abs/1511.00000)

---

## Contents

<b>1</b>	<b>Introduction</b>	<b>1</b>
<b>2</b>	<b>Particle origin and Cosmology of LFDM and ULA DM</b>	<b>2</b>
2.1	LFDM	2
2.2	ULA dark matter	3
<b>3</b>	<b>Simulating the reionization field</b>	<b>4</b>
3.1	Generating the dark matter density field	4
3.2	Identifying collapsed dark matter halos	5
3.3	Generating the neutral hydrogen (HI) maps	6
<b>4</b>	<b>Results</b>	<b>7</b>
<b>5</b>	<b>Evolution of cosmological gas density</b>	<b>10</b>
<b>6</b>	<b>Conclusion</b>	<b>12</b>

---

## 1 Introduction

After intensive searches over decades, the nature of dark matter is still a mystery. This strange type of matter reveals its presence only through gravitational interaction in astrophysics and cosmology. The existence of dark matter is very well confirmed by various observations covering many length scales and epochs of our universe. Some examples are the cosmic microwave background anisotropy experiments[1–3], large scale structure surveys[4, 5], study of the galaxy rotation curve[6], cosmological weak gravitational lensing observations[7] etc. Though all of these experiments have confirmed the existence of dark matter, they do not throw any light on its fundamental nature. One of the leading candidate of dark matter, the Weakly Interacting Massive Particle (WIMP) or the traditional cold dark matter (CDM), is inspired by the well known WIMP miracle. This WIMP miracle relies on the coincidence between weak scale cross-section and the dark matter freeze-out cross-section needed to produce correct relic density. This discovery has driven a lot of direct[8–12], indirect[13–21] and collider[22, 23] searches but these experiments have not yet succeeded in determining the particle nature of dark matter. In fact, the results from many of these experiments are found to be in conflict[24] with each other.

In addition, there exists some long standing cosmological problems with WIMPs. One of them is the **cuspy-core** problem[25], indicated by the discrepancy between increasing dark matter halo profile (cusp) towards the center of galaxy from N-body simulation [26] and the observationally found relatively flat density profile [27]. It is instructive to note that though there exist difference in opinions about cuspy-core issue of CDM and dwarf galaxy observations [28]. Another issue with WIMPs is the missing satellite problem[29, 30] where N-body simulations of structure formation with CDM produce a lot more satellite haloes of a Milky-Way type galaxies than observed. The “too big too fail”[31, 32] problem, another thorn in the crown of  $\Lambda$ CDM model, shows that the majority of the most massive subhaloes of the Milky Way are too dense to host any of its bright satellites. Some recent works claim that these issues may persist even when the impact of small scale baryonic physics is included [33–35]. All these issues have inspired a drive to go beyond the standard WIMP picture of CDM and consider alternative candidates for dark matter, which differ from CDM on galactic scales (while reproducing its success on cosmological scales).

One such alternative is the warm dark matter (WDM), which causes a decrement in the matter power at small scales[36, 37] due to a larger free-streaming distance than CDM and may provide a solution to some of the small-scale problems [38]. But such models are not without issues. The N-body simulation of WDM is very sensitive to WDM mass and it tends to produce fewer number of satellites than already observed[39–41]. The status of the cuspy-core problem has improved[42, 43] but unfortunately it is not fully resolved by introducing the WDM. In addition WDM has issues with Lyman- $\alpha$  forest flux power spectrum [37] where

observational results, combined with hydrodynamic simulations of structure formation place the strongest constraint to date on WDM mass  $m_W \geq 3.3$  keV [44]. But the preferred mass range that arises from WDM N-body simulation is different. It was shown in [42] that the solution to the **cusp-core** problem requires WDM particles with mass  $m_W \sim 0.1$  keV. It has also been pointed out that WDM particles with mass in the range  $1.5 \text{ keV} \leq m_W \leq 2 \text{ keV}$  can solve the too-big-to-fail problem [41]. In this work we investigate two models of dark matter that result in WDM-like suppression in power at small scales but their physical origin and nature of power spectra at small scale is significantly different from WDM models.

We focus on two models of dark matter—namely “Late Forming Dark Matter (LFDM)” and “Ultra Light Axion (ULA)” dark matter. The former has its origin in extended neutrino physics [45] while the later originates from string theory [46]. In Both of these cases, dark matter starts behaving as CDM after the epoch of BBN and before the epoch of matter radiation equality and both of them have similar features (oscillations and suppression in small scale power) in matter power spectra. Given the similarities between the ULA and LFDM models, it is reasonable to expect that in some viable region of the ULA parameter space, the two models may share the same phenomenology of the matter clustering at small scale. Indeed a recent N-body simulation work on LFDM [47] and two simulations for ULA DM [48–50] have shown that these models appear to offer a good solution to cusp-core issue while being consistent with large scale clustering.

In this paper, we study the effects of these dark matter models on two distinct features of the universe. The first one is the Epoch of Reionization (EoR). This epoch is one of the most important milestone of the history of the universe, though one of the least well understood. From QSO absorption studies and CMB anisotropy measurements we know the reionization occurred at  $z \simeq 9$  even though it could be an extended process lasting until  $z \simeq 6.5$  [51, 52]. The details of EoR are sensitive to the collapsed fraction of baryons which in turn depends on the matter power spectrum at small scales (see e.g. [53]). In particular, we study the impact of LFDM and ULA models on the HI signal from the EoR. Another direct probe of the suppression in power at small scales is the evolution of collapsed fraction at high redshifts. The Damped Lyman- $\alpha$  data, based on absorption studies, in the redshift range  $2 < z < 5$  can be used to construct the evolution of the total amount of HI in bound objects [54–57], which provides a lower limit to the collapsed fraction of matter in this redshift range.

To constrain LFDM and ULAs using EoR, one needs the dark matter distribution at high redshift  $z = 8$ . We have used a particle-mesh N-body code [58, 59] to evolve the initial matter power spectra of LFDM and ULA DM models from  $z = 124$  to  $z = 8$ . This is how WDM simulations are also studied [39–41] in the literature and is valid on scales above the present-day Jeans scales of these models. It is important to check the validity of this procedure for LFDM and ULA DM. This has been done in [47, 48]. It is instructive to note that these simulation will not resolve the internal halo structure. For ULAs, this could be achieved using a wave-like simulation following the method of [48]. But for the purpose this paper, our approach is accurate enough to confront LFDM and ULA models from the Epoch of Reionization (EoR) observations.

The paper is organized as follows. In Section 2, we provide a brief description about the particle nature of the LFDM and ULAs along with its cosmological effects on the matter power spectrum. In section 3, we provide the details of the simulation set-up for the reionization field. In section 4, we present the results of our simulations including the predictions for the HI power spectrum. In section 5, using analytical models for mass function, we study the effect of our models on the evolution of cosmological gas density and compare our results with damped Lyman- $\alpha$  observations. Section 6 is reserved for concluding remarks.

Throughout this paper, we have used the Planck+WP best fit values of cosmological parameters:  $\Omega_{m0} = 0.3183$ ,  $\Omega_{\Lambda 0} = 0.6817$ ,  $\Omega_{b0} h^2 = 0.02203$ ,  $h = 0.6704$ ,  $\sigma_8 = 0.8347$ , and  $n_s = 0.9619$  [1, 51].

## 2 Particle origin and Cosmology of LFDM and ULA DM

### 2.1 LFDM

Here, we consider a scenario in which the DM is consequence of a phase transition in the dynamics of a scalar field [45, 60]. There can be two types of LFDM: Bosonic and Fermionic. The bosonic or scalar LFDM forms when a scalar field  $\phi$  (coupled with massless neutrino), trapped in the false vacuum of potential  $V(\phi)$ , makes transition to the true vacuum during the evolution of the universe and starts behaving like dark matter. In case

of Fermionic LFDM, the freely propagating massless neutrinos get trapped into small nuggets by some fifth force [61] and the nuggets start behaving like dark matter. But as both of these two types of LFDM gets their initial condition from standard model neutrino, we don't expect to see any difference in the evolution of the universe. These models have been studied by [60] and it is found that the dark matter must form deep inside the radiation dominated era. The small scale effects of LFDM is studied in [47] using  $N$ -body simulations.

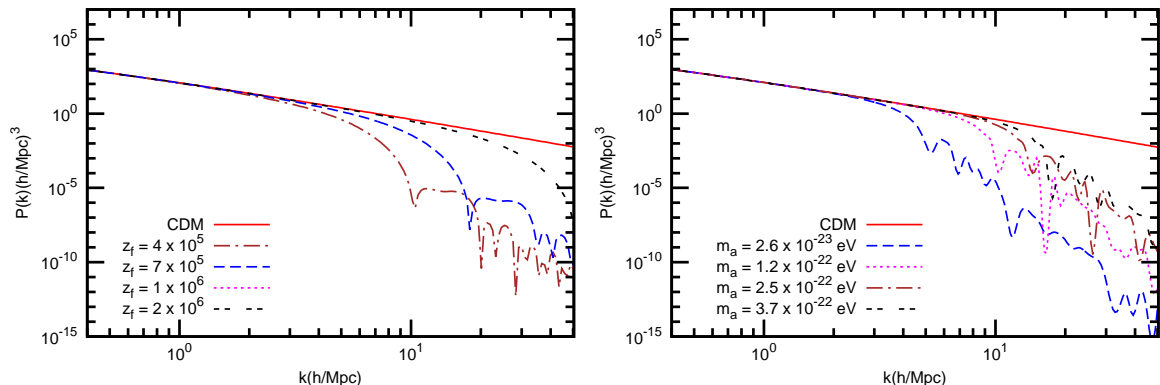


**Figure 1.** Normalized power spectra for LFDM models with different  $z_f$  (Left panel) and ULA models with different masses (Right Panel)

There are two main features of LFDM cosmology that manifest themselves in the matter power spectra. First, there is a sharp break in the power at the co-moving scale  $k_e = aH_e$ ; where  $H_e$  is the Hubble scale at the epoch of phase transition  $z_f$ . Second, there are damped oscillations at smaller scales. Both of these can be seen in Figure 1, in which we show the normalized power spectra for LFDM models for many four different values of  $z_f$ . The details of the computation of this power spectrum are provided in [60].

The nature of the power spectrum can be understood as follows. Before the phase transition, due to strong coupling with massless neutrinos, the density and velocity perturbations of the scalar field follow that of the neutrino. On the super horizon scales, the massless neutrinos behave like other forms of matter such as the CDM. However the perturbations in this component are washed out owing to free-streaming on scales smaller than the horizon at  $z = z_f$ . The complete solution for the density perturbation is an exponentially damped oscillation at sub-horizon scales. The scales smaller than  $k_e$ , i.e the scale which enters the horizon at the time of transition, are thus expected to carry the signature of the behavior of massless neutrino as LFDM obtains its initial conditions from them. After the transition, the scalar field decouples from the neutrino and starts behaving like CDM. It can be noted in Figure 1 that this is exactly how LFDM power spectrum behaves for  $k > k_e$ . As  $z_f$  is increased the feature shifts to larger  $k_e$ , or smaller scales. As  $z_f$  tends to infinity, the LFDM matter spectrum approaches the  $\Lambda$ CDM results.

## 2.2 ULA dark matter

Another candidate for dark matter with novel effects on galactic scales which is also well studied in recent past is the dark matter from ultra light axion like particles (ULAs) [48, 62–70]. For a recent review on this, see Refs.[50]. In this case, there are ultra-light axions with mass as low as  $10^{-18} - 10^{-33}$  eV which has their well motivated origin is string axiverse scenario [46]. They can play the role of dark matter at late time when the axion field overcome the Hubble friction and starts oscillating coherently in a quadratic potential. This dark matter from ULA are similar to the well known QCD axion DM. The only difference being that the mass of these particle is much lower than QCD axion and thus the dark matter behavior happens at much late time when Hubble parameter drops below the mass of ULAs. ULAs with smaller mass start behaving as dark matter later.

ULAs are created by spontaneous symmetry breaking and behave as a coherent classical scalar field. It obtains its initial condition after symmetry breaking in the early universe. Unlike LFDM it remains frozen at this initial value by Hubble drag and behaves like a cosmological constant as long as  $H(t) > m_a$  where  $m_a$  is the axion mass. When the Hubble parameter drops below  $m_a$ , the field begins behaving like cold dark

matter. Below a certain scale determined by a momentum-dependent effective sound speed of the perturbation in the scalar field, the particle free-streaming leads to suppression of growth of structures [62, 65, 66, 70]. This suppression is indicated as a sharp break in the matter power spectra at the corresponding Jeans scale as shown in Figure 1. The Jeans scale is given by [50]

$$k_J = 66.5 a^{\frac{1}{4}} \left( \frac{\Omega_a h^2}{0.12} \right)^{\frac{1}{4}} \left( \frac{m_a}{10^{-22}} \right)^{\frac{1}{2}} \text{Mpc}^{-1}. \quad (2.1)$$

and after some simplification it can be shown that the suppression of structure formation in the matter dominated era occurs below a scale [66]:

$$k_m \sim \left( \frac{m}{10^{-33} \text{eV}} \right)^{1/3} \left( \frac{100 \text{ kms}^{-1}}{c} \right) h \text{Mpc}^{-1}. \quad (2.2)$$

This means that the lesser the axion mass the larger the suppression scale as can be seen from Figure 1. For the least massive ULA used in this work, the above relation yields  $k_m \sim 1 h \text{Mpc}^{-1}$ . This Jeans scale in linear power spectra has a considerable effect on CMB physics and ULA can also be constrained from large scale structure surveys. The cosmologically relevant mass range for ultra light axion is given by  $10^{-33} \text{eV} < m_a < 10^{-18} \text{eV}$  [50]. recently, using Planck and WiggleZ data and linear physics alone Hlozek et al [63] essentially excludes mass range below  $m_a < 10^{-24}$  if ULA constitutes the whole of dark matter. In this work, we are interested in ULAs with masses  $\gtrsim 10^{-23}$  eV which suppress structure formation on scales comparable WDM with  $m_W \gtrsim 0.1 \text{keV}$

### 3 Simulating the reionization field

The redshift evolution of the mass averaged neutral fraction  $\bar{x}_{\text{HI}}$  during EoR is largely unknown. It is only constrained from the CMB anisotropy and polarization measurements (ref. ) which allow us to infer the optical depth integrated through the reionization surface. Therefore, the CMB constraints can be satisfied for a wide range of ionization histories [71].

Our aim here to study the HI signal from the reionization era for a class of LFDm and axion models and, if possible, discern generic features of such models from the HI power spectra. Given the uncertainty of reionization history, we do not assume a particular model for reionization history  $\bar{x}_{\text{HI}}(z)$ . Instead we fix the redshift and the ionization fraction at which these models are compared. We take  $z = 8$  and  $\bar{x}_{\text{HI}} = 0.5$  at this redshift for our simulations.

Our method of constructing reionization fields consists of three steps: (i) generating the dark matter distribution at the desired redshift, (ii) identifying the location and mass of collapsed dark matter halos within the simulation box, (iii) generating the neutral hydrogen map using an excursion set formalism [72]. The assumption here is that the hydrogen exactly traces the dark matter field and the dark matter halos host the ionizing sources<sup>1</sup> We discuss our method in the following sections.

#### 3.1 Generating the dark matter density field

We have used a particle-mesh  $N$ -body code [58] to simulate the  $z = 8$  dark matter distribution. We use the linear power spectrum (Figure 1) to generate the initial Gaussian random density field at  $z = 124$ . For LFDm, the linear power spectra are generated using a modified version of CAMB [60] and axionCAMB is used for the ULA dark matter [63]. We have done simulations for the following models:  $\Lambda$ CDM, LFDm models with  $z_f = \{2, 1, 0.7, 0.4\} \times 10^6$ , and ULA models with  $m_a = \{3.7, 2.5, 1.2, 0.26\} \times 10^{-22} \text{eV}$ . Figures 2 shows

<sup>1</sup>The assumption that the dark matter follows the baryons is justified for simulating the HI signal from EoR for the following reasons. The issue of simulating and studying this signal is essentially a two-scale problem: the scale at which the structures collapse and the scale at which the HI signal is observable. These scales are generally separated by orders of magnitude. For instance, the objects that collapse around  $z \simeq 10$  lie in the mass range  $M \simeq 10^9 - 10^{10} M_\odot$ , which correspond to length scales  $L \simeq 0.2 - 0.4 \text{Mpc}$  or equivalently  $k \simeq 2\pi/L \simeq 30 - 15 \text{Mpc}^{-1}$ . However, we study the HI signal in the range  $0.1 < k < 4 \text{Mpc}^{-1}$ . So even though the density field is highly non-linear at the scale of the collapse and therefore the assumption that baryons follow dark matter is not a good one, it generally is an excellent assumption at the scales at which the HI is probed, which lie in the range from mildly non-linear to highly linear at the redshifts of interest.

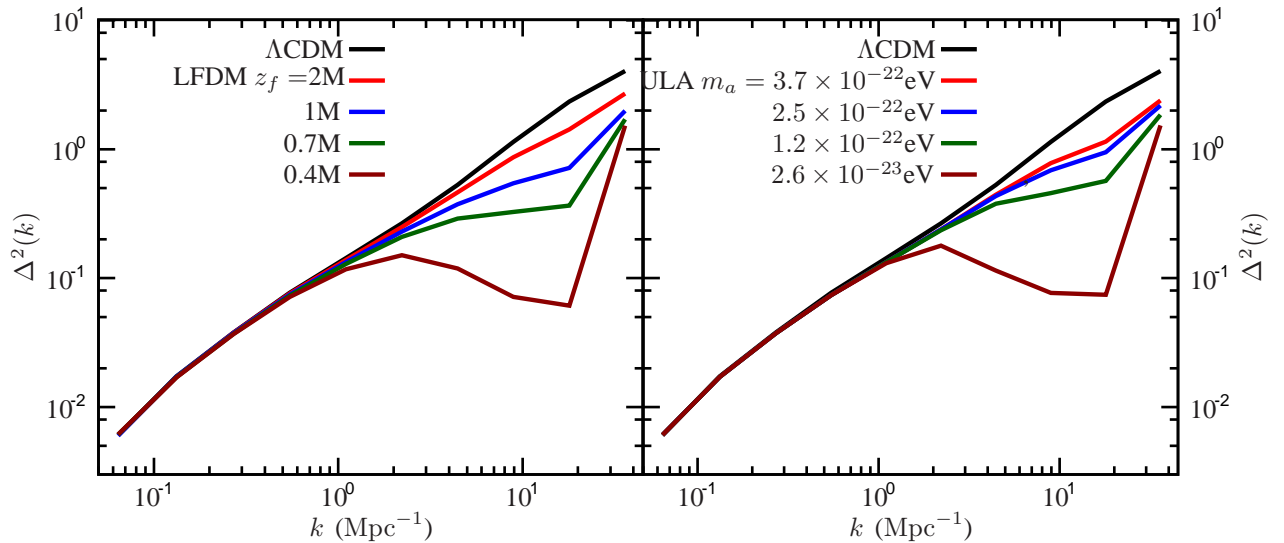


**Figure 2.** This shows the dimensionless matter power spectrum  $\Delta^2(k)$  at  $z = 8$  calculated from the  $N$ -body outputs using four different LFD models (left panel) with  $z_f = \{2, 1, 0.7, 0.4\} \times 10^6$  and four different axion DM models (right panel) with axion masses  $m_a = \{3.7, 2.5, 1.2, 0.26\} \times 10^{-22}$  eV. The black solid curves are the  $\Lambda$ CDM power spectrum.

the dimensionless matter power spectrum  $\Delta^2(k) = k^3 P(k)/2\pi^2$  output from the  $N$ -body simulation at  $z = 8$ . Note the suppression of power on scales  $k \gtrsim 1 \text{ Mpc}^{-1}$  for both the LFD (left panel) and ULA (right panel) models compared to the  $\Lambda$ CDM model. This suppression deepens as we decrease the value of  $z_f$  and  $m_a$  in the LFD and ULA models respectively.

Our simulation volume is a  $[150 \text{ Mpc}]^3$  comoving box. We have run our simulation with a  $2144^3$  grid using  $1072^3$  dark matter particle. The spatial resolution is  $0.07 \text{ Mpc}$  which corresponds to a mass resolution of  $1.09 \times 10^8 M_\odot$ . The  $N$ -body code used for this work has been parallelized [73] for shared-memory machines using OpenMP.

### 3.2 Identifying collapsed dark matter halos

We have used a friends-of-friends (FoF) halo finder code [59] to identify the location and mass of the collapsed dark matter halos from the outputs of the  $N$ -body simulation. We have used a fixed linking length 0.2 times the mean inter-particle separation and require a halo to have at least 10 dark matter particles which corresponds to a minimum halo mass of  $1.09 \times 10^9 M_\odot$ . Our choice of minimum halo mass is also fair because a halo mass of few times  $10^8 M_\odot$  [74] (at  $z = 8$ ) also corresponds to the virial temperature ( $\sim 10^4 \text{ K}$ ) of hydrogen cooling threshold.

Figure 3 shows the simulated comoving number density of halos per unit logarithmic halo mass  $dn/d(\ln M)$  as a function of the halo mass  $M$  at  $z = 8$  for the range of LFD (left panel) and ULA (right panel) models that we consider here. The solid curve is the theoretical  $\Lambda$ CDM mass function [75]. The simulated  $\Lambda$ CDM mass function, shown in black points, is in very good agreement with the theoretical mass function. Note that the low mass halo abundance is substantially reduced for both the LFD and the ULA models as compared to the  $\Lambda$ CDM, and the suppression gets steeper with decreasing value of  $z_f$  and  $m_a$  in the LFD and ULA models respectively.

In the right panel of Figure 3, we also show the theoretical halo mass function for ULAs of Ref. [68]. The theoretical mass function displays a sharp cut-off at low halo masses caused by scale dependent growth and an increased barrier for collapse: consequences of the ULA Jeans scale. This cut-off is not present in the mass function found from our  $N$ -body simulations, but we should not expect it to be.  $N$ -body simulations treat ULAs as particles. However, this treatment is incomplete on small scales, where the coherent scalar field dynamics become important. The full scalar field dynamics have been computed by Ref. [48], and the validity of an  $N$ -body treatment on large scales was discussed in Ref. [76]. The cut-off in the theoretical mass function for ULAs becomes relevant precisely where scale dependent growth and scalar field dynamics become important

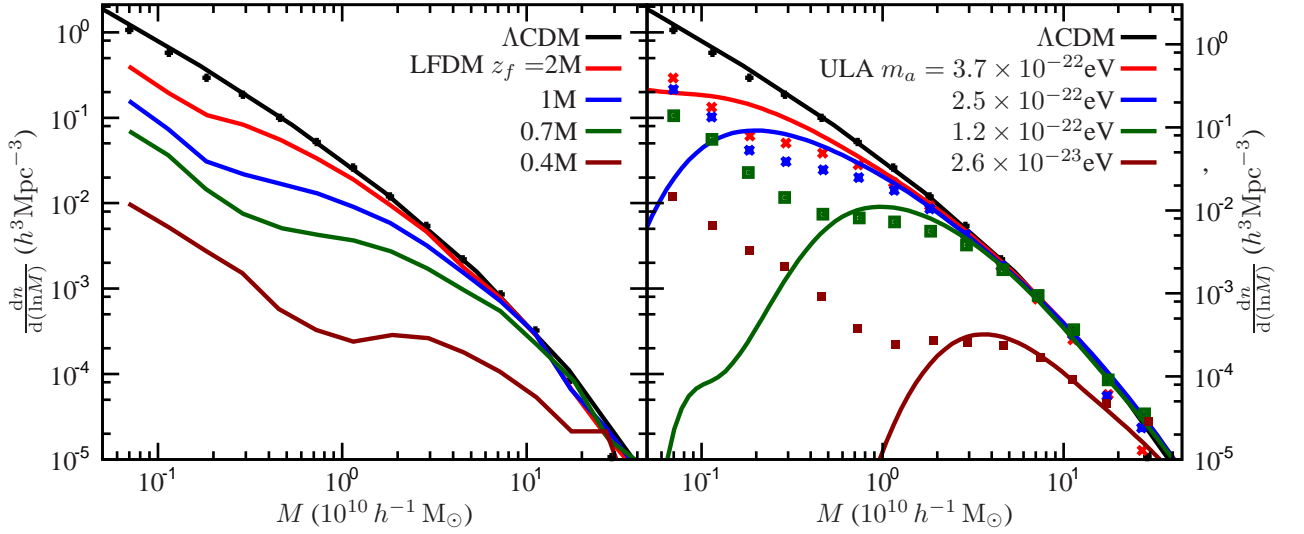


**Figure 3.** This shows the halo mass function from our simulations considering four different LFDM models (left panel) with  $z_f = \{2, 1, 0.7, 0.4\} \times 10^6$  and four different axion DM models (right panel) with axion masses  $m_a = \{3.7, 2.5, 1.2, 0.26\} \times 10^{-22}$  eV. The black soiled curve is the theoretical  $\Lambda$ CDM mass function of Ref. [75]. In the right hand panel, the points represent the results of the simulation, while the solid curves are the theoretical prediction from [68].

in linear theory. This suggests that the ULA mass functions we have derived should not be considered correct on these scales.

Both the LFDM and ULA mass functions produce low mass halos below the cut-off in the linear theory power spectrum. The same effect is observed in related simulations of warm dark matter (WDM). In the case of WDM, these low mass halos are believed, for a variety of reasons, to be “spurious” [77, 78]. We note that for ULAs the mass function slope from simulations increases below the cut-off in the theoretical mass function. An increase in the slope of the mass function is one method of identifying spurious halos [79], and it is interesting that these scales coincide. A complete simulation of ULAs (either as a scalar field [48], or an effective fluid [49, 80]) should include a dynamical mechanism whereby the spurious halos never form, thanks to the so-called “quantum pressure” of the gradient energy. This further suggests, on theoretical grounds, that the low mass halos are spurious.

Spurious structure can be removed from simulated mass functions: for WDM in e.g. Ref. [79], for LFDM in Ref. [81], and for ULAs in Ref. [76]. In our results we do not remove the spurious structure. The constraints thus derived will be weaker than the true constraints, allowing for lighter ULAs and later formation of DM. Our constraints are therefore, in some sense, conservative.

### 3.3 Generating the neutral hydrogen (HI) maps

In the final step we generate the ionization map and the HI distribution using the homogeneous recombination scheme of Ref [82]. The basic assumption here is that the hydrogen exactly traces the matter density field and the halos host the sources of ionizing photons. It is also assumed that the number of ionizing photons emitted by a source  $N_\gamma$  is proportional to the mass of the host halo *i.e.*  $N_\gamma = N_{\text{ion}}M/m_p$  where  $m_p$  is the proton mass. The constant of proportionality  $N_{\text{ion}}$  here is the number of ionizing photons emitted per baryon in the collapsed halo times the ratio of the baryon density to the total matter density. The ionization map is generated by comparing the smoothed photon number density to the smoothed hydrogen number density at each grid point in the simulation volume. Any grid point where the photon number density exceeds the hydrogen number density is declared to be ionized. This comparison is carried out varying the smoothing radius from the cell size to a maximum smoothing length-scale which is half the box size. The ionized map and the HI distribution were generated using a grid spacing that is 8 times coarser than the  $N$ -body simulations. The simulated HI distribution was finally mapped to redshift space ([83]) using the scheme outlined in Ref. [84].

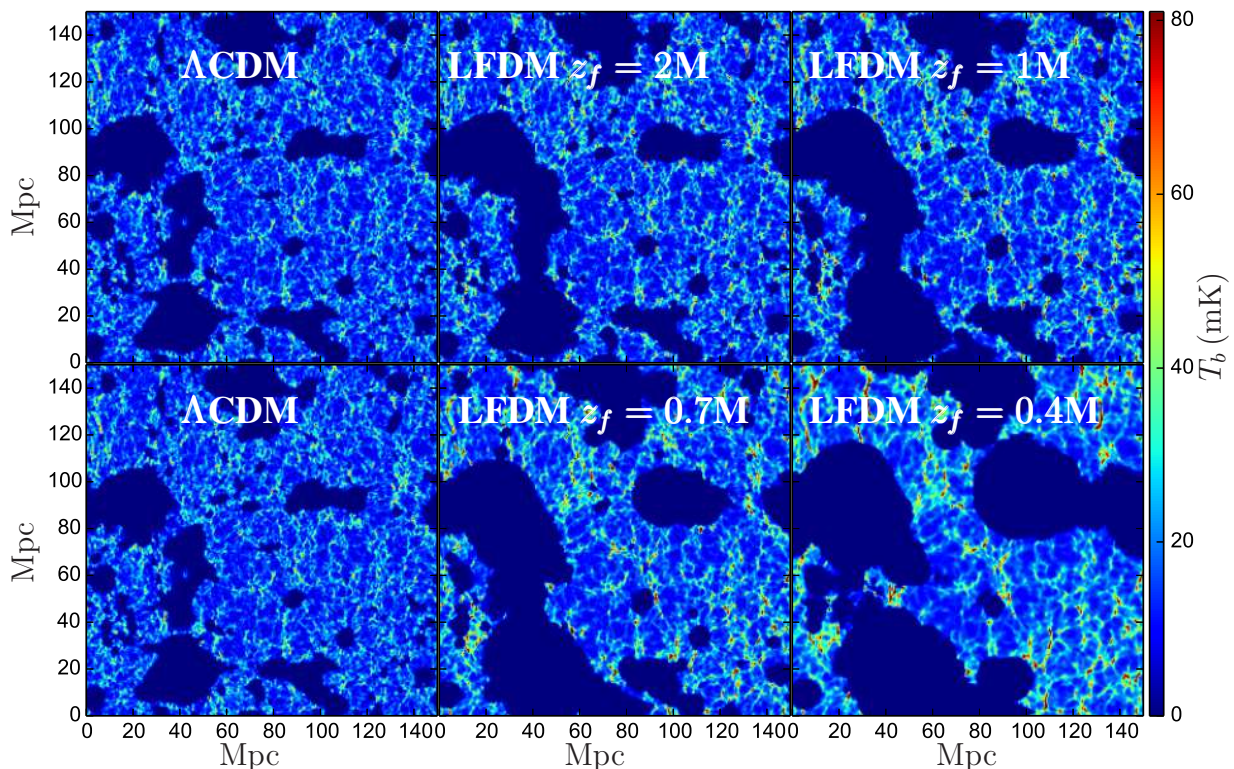


**Figure 4.** Two dimensional sections through the simulated brightness temperature maps of four LFD models along the  $\Lambda$ CDM model for  $\bar{x}_{\text{HI}} = 0.5$ . The  $\Lambda$ CDM (left) map has been shown twice. The direction of redshift space distortion is with respect to a distant observer located along the vertical axis.

We use the resulting HI distribution to calculate the brightness temperature fluctuation using ([85])

$$\delta T_b = 4\text{mK} \frac{\rho_{\text{HI}}}{\bar{\rho}_{\text{H}}} (1+z)^2 \left( \frac{\Omega_b h^2}{0.02} \right) \left( \frac{0.7}{h} \right) \frac{H_0}{H(z)}, \quad (3.1)$$

where  $\frac{\rho_{\text{HI}}}{\bar{\rho}_{\text{H}}}$  is the ratio of the neutral hydrogen to the mean hydrogen density. Throughout this paper, we assume the spin temperature  $T_s \gg T_{\text{cmbr}}$  or the HI is only observed in emission.

## 4 Results

Our method predicts an ‘inside-out’ ionization where the high density regions are ionized first and the low density region later. As the value of  $z_f$  in LFD model decreases, the number of halos decreases. This means that the number of ionizing sources in the LFD and ULA models is smaller as compared to  $\Lambda$ CDM model. To achieve the same ionization level at the same redshift ( $\bar{x}_{\text{HI}} = 0.5$ ),  $N_{\text{ion}}$  is higher in the LFD models as compared to the  $\Lambda$ CDM model. We find that for  $z_f < 0.4 \times 10^6$  the desired level of reionization doesn’t occur as we couldn’t form dark matter halos in our box. This allows us to put a rough limit of  $z_f \sim 0.4 \times 10^6$  as a lower cut off. Similar considerations allows us to put a lower limit on the mass of ULA of  $m_a > 2.6 \times 10^{-23}$  eV. It is instructive to note that this result is consistent with [63, 76] in connection to linear as well as non-linear observables of ULA DM. Table 1 lists the set of models we study in this paper.

However, we could also get independent limit on  $z_f$  and  $m_a$  from constraints on plausible range of  $N_{\text{ion}}$ . In our simulation  $N_{\text{ion}} = 24$  for the  $\Lambda$ CDM model. For the range of LFD models we have studied (for decreasing  $z_f$  as shown in Figure 4):  $N_{\text{ion}} = \{47, 102, 212, 1230\}$ . For ULA models, for decreasing  $m_a$  as shown in Figure 5,  $N_{\text{ion}} = \{61, 75, 134, 965\}$ . Table 1 lists the values of  $N_{\text{ion}}$  for the models we consider.

How acceptable are these values if star-forming galaxies were responsible for the reionization process? For a metallicity  $Z = 0.01$  and Scalo stellar mass function, the number of hydrogen ionizing photons is nearly

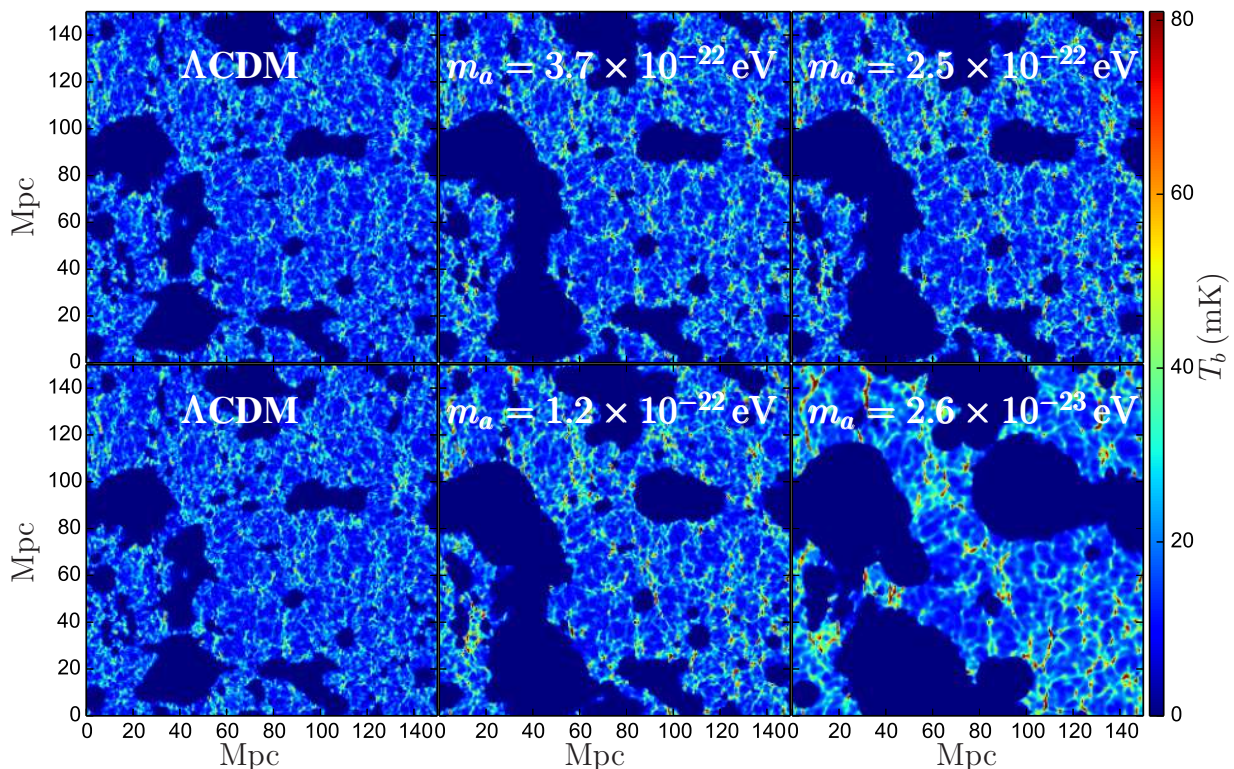


**Figure 5.** Two dimensional sections through the simulated brightness temperature maps of the four different axion DM models with axion masses  $m_a = 3.7 \times 10^{-22}$  eV,  $2.5 \times 10^{-22}$  eV,  $1.2 \times 10^{-22}$  eV and  $2.6 \times 10^{-23}$  eV for  $\bar{x}_{\text{HI}} = 0.5$ . The  $\Lambda\text{CDM}$  (left) map has been shown twice. The direction of redshift space distortion is with respect to a distant observer located along the vertical axis.

4000 per baryon which corresponds to  $N_{\text{ion}} \simeq 800$ . Factoring in 10% star formation efficiency in a halo for star forming galaxies and 10% escape fraction from these haloes, this number drops by a factor of 100.<sup>2</sup> It should be noted that all these factors—metallicity, initial mass function, star formation efficiency, and escape fraction—are highly uncertain. For zero metallicity (population III) stars the number of photons could be significantly higher and lie in the range  $10^4$ – $10^5$ <sup>3</sup>, but these stars last only a few million years which is considerably smaller than the age of the universe,  $\simeq 5 \times 10^8$  yrs at  $z \simeq 8$ . These first metal-free, massive stars would have ended their life in supernova explosions thereby contaminating the interstellar medium with metals. This means the metal-free stars could only have dominated the reionization process for short periods. Also for initial stellar mass functions which have a larger fraction of massive O and B stars as compared to the Scalo mass function, the number of ionizing photons could be larger (for details of the physics of ionizing sources during the epoch of reionization see [53]).

In light of these facts we could ask how plausible is  $N_{\text{ion}}$  corresponding to  $z_f \simeq 0.4 \times 10^6$  or  $m_a \simeq 2.6 \times 10^{-23}$  eV. In these cases, the required number of photons per baryon is larger than 5000. This is not possible to achieve for moderate metallicities and Scalo mass function even if the efficiency of star formation and the escape fraction are 100%. Therefore, we consider such models unrealistic.

Upcoming near-infrared telescope JWST will allow us to directly detect ionizing sources from the epoch of reionization (e.g. Figure 19 of [53]). For LFDm and ULA models, these sources are fewer in number and more luminous, which might allow a direct probe of the decrement of matter power spectra at small scales.

<sup>2</sup>We note that the effective number of hydrogen ionizing photons in the case of early QSOs where these photons are produced owing to the conversion of gravitational energy into energy are comparable to the case of early star-forming galaxies [53].

<sup>3</sup>From current observations it is difficult to constrain the fraction of PopIII stars during the epoch of reionization but plausible bounds based on the observed Infra-red background and its fluctuations suggest PopIII stars might not have dominated the reionization process [86, 87]

Model	Parameter	$N_{\text{ion}}$	Reionization
CDM	[1, 51]	24	✓
LFDM	$z_f = 2.0\text{M}$	47	✓
	$z_f = 1.0\text{M}$	102	✓
	$z_f = 0.7\text{M}$	212	✓
	$z_f = 0.4\text{M}$	1230	×
	$z_f = 0.2\text{M}$	No Haloes	×
ULA DM	$m_a = 3.7 \times 10^{-22}\text{eV}$	61	✓
	$m_a = 2.5 \times 10^{-22}\text{eV}$	75	✓
	$m_a = 1.2 \times 10^{-22}\text{eV}$	134	✓
	$m_a = 2.6 \times 10^{-23}\text{eV}$	965	×
	$m_a = 2.0 \times 10^{-23}\text{eV}$	No Haloes	×

**Table 1.** The Table lists the values of  $N_{\text{ion}}$  for the LFDM and ULA models we consider. In the last column the tick mark illustrates whether the models is able to achieve reionization based on an acceptable value of  $N_{\text{ion}}$  and the formation of haloes in the N-body simulation.

Figures 4 and 5 show two-dimensional sections through the simulated brightness temperature cubes for LFDM and ULA models for  $\bar{x}_{\text{HI}} = 0.5$ . By visual comparison we see two main differences between  $\Lambda\text{CDM}$  and LFDM (ULA) models. The first difference is that the size of the ionized regions is larger in the LFDM (ULA) models. It is owing to two factors: first, as discussed above, it is a consequence of the fact that the sources require higher star formation efficiency to achieve the desired level of ionization. Second, the suppression of matter power at small scales results in a decrement of mass dispersion at these scales. Therefore, the haloes that form are a higher  $\sigma$  fluctuations of the density field as compared to the  $\Lambda\text{CDM}$  model. It is known that higher  $\sigma$  fluctuations are more strongly clustered for a Gaussian field (see e.g. [88, 89]), or the ionizing sources are formed more preferentially in a cluster. Both these factors contribute to enlarging the size of the ionizing bubble and explain why the ionized bubble sizes get larger with decreasing value of  $z_f$  ( $m_a$ ) in the LFDM (ULA) models. The second difference, also linked to the factors discussed above, is that the HI fields has stronger contrast in the LFDM models. Both these differences manifest themselves in the power spectra of the HI field which we discuss next.

Figures 6 shows the mean squared brightness temperature fluctuation  $\Delta_b^2(k) = k^3 P_b(k)/2\pi^2$  of the HI field for LFDM (left panel) and ULA (right panel) models we consider here along with the  $\Lambda\text{CDM}$  model, for a fixed ionization fraction  $\bar{x}_{\text{HI}} = 0.5$ . We find that the power for LFDM (ULA) models is greater than the  $\Lambda\text{CDM}$  model over a large range of scales  $0.1 < k < 4 \text{Mpc}^{-1}$ . This is owing to the factors discussed in the foregoing. The scale of the HI power spectra from ionization inhomogeneities, is governed by the size of ionized bubbles. These inhomogeneities normally dominate the contribution of density perturbations for scales considered here. Therefore we expect, for the same ionized fraction, the power to increase if the ionized bubbles are larger. It has been shown analytically [72] and is consistent with the results of numerical simulations [90]. Conversely, when there is enhancement of matter power at small scales, e.g. owing to the presence of primordial magnetic fields, the HI signal in the range of scale discussed here, diminishes [91].

We only consider a fixed ionization fraction  $\bar{x}_{\text{HI}} = 0.5$  at  $z = 8$  for our study. However, the discussion in the foregoing shows that the enhancement of the HI signal is generic and should be independent of the ionization fraction. It can be shown that the HI signal is dominated by ionization inhomogeneities and it peaks at close to  $\bar{x}_{\text{HI}} = 0.5$  [72], which also partly motivates our choice.

Current observational constraints from radio interferometer PAPER put an upper limit on the HI bright

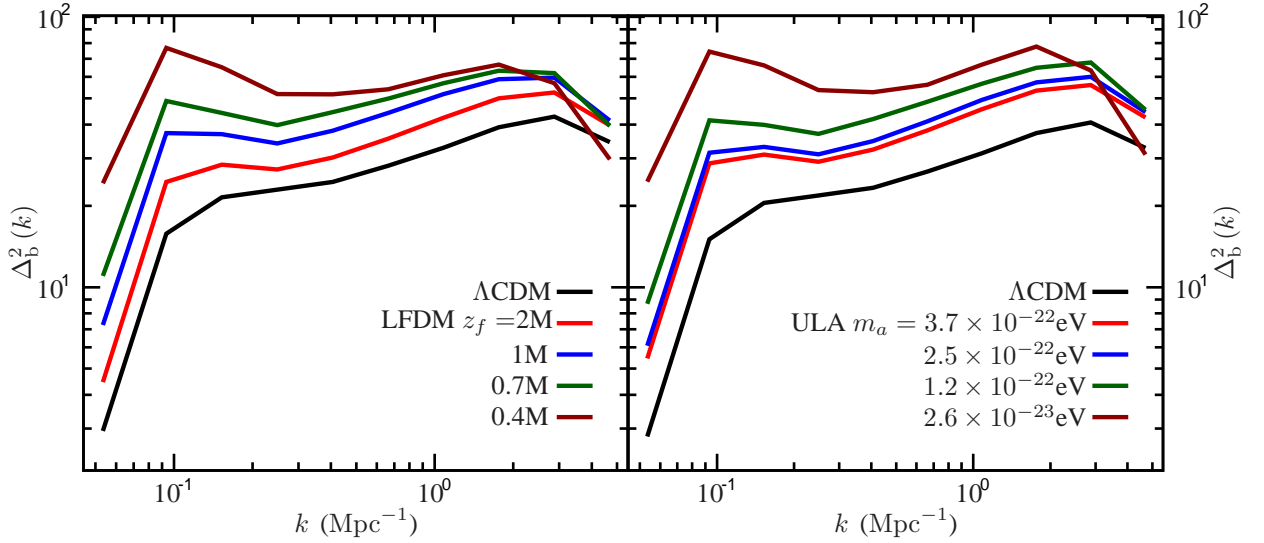


**Figure 6.** This shows the brightness temperature power spectrum  $\Delta_b^2(k)$  ( $\text{mK}^2$ ) of the HI field for the four different LFD models (left panel) with  $z_f = \{2, 1, 0.7, 0.4\} \times 10^6$  and four different axion DM models (right panel) with axion masses  $m_a = \{3.7, 2.5, 1.2, 0.26\} \times 10^{-22}$  eV. The black solid curves are for the  $\Lambda\text{CDM}$  model.

temperature power spectrum:  $\Delta_b^2(k) < (22.4\text{mK})^2$  over the range of scales  $0.15 < k < 0.5\text{kMpc}^{-1}$  at  $z = 8.4$  [92]. These constraints are too weak, by roughly a factor of 10, to probe the enhancement of the HI signal seen in Figure 6 for LFD and ULA models at the present. Ongoing radio interferometers focused on detecting the HI signal from EoR—LOFAR, MWA, and PAPER—might throw more light on this issue in the near future.

## 5 Evolution of cosmological gas density

As discussed in the previous section, the main impact of LFD and ULA models is to reduce the matter power at small scales. This results in smaller number of haloes at masses relevant for studying the reionization process. This also means the collapsed fraction of matter decreases for models with lower power. We study the implication of the evolution of the collapsed fraction for LFD and Axion models in this section.

From absorption studies of Damped Lyman- $\alpha$  clouds, the evolution of average mass density of HI in the universe can be inferred [54, 55]. Assuming that the HI follows baryons and the collapsed fraction of baryons traces dark matter, this allows us to get an approximate measure of the minimum amount of collapsed fraction of the total matter in the redshift range  $2 < z < 5$  for which the data are available [54, 56, 57]. From the HI data one obtains,  $\Omega_{\text{HI}}(z) = \rho_{\text{HI}}^{\text{coll}}(z)/\rho_c(z)$ , which gives the fraction of the collapsed neutral hydrogen in terms of critical density of the universe  $\rho_c$ . The (minimum) collapsed fraction is given by:  $f_{\text{coll}}(z) = \rho_c(z)/\rho_b(z)\Omega_{\text{HI}}(z)$ , where  $\rho_b$  is the background energy density of Baryons.

As obtaining the mass function from N-body simulation is numerically expensive, for computing the collapsed fraction, for LFD models, we integrate the Sheth-Tormen mass function [75, 93] above the density threshold of collapse at a given redshift. The collapsed fraction (the fraction of collapsed mass in haloes with masses larger than  $M$ ) at a redshift  $z$  is given by:

$$f_{\text{coll}}(M, z) = \int_{\nu_{\text{min}}}^{\infty} \nu f(\nu) \frac{d\nu}{\nu} \quad (5.1)$$

Here  $\nu_{\text{min}} = (1.69/\sigma(M, z))^2$  and  $f(\nu)$  is given by the Sheth-Tormen mass function [75, 93]. For computing the collapsed fraction for ULA models, we integrate the halo mass functions derived by [68].

In Figures 7 and 8 we show the mass dispersion  $\sigma(M)$  for a range of LFD and ULA models and collapsed fraction as a function of mass for a fixed redshift. It is seen that as the formation redshift  $z_f$  ( $m_a$ )

decreases,  $\sigma(M)$  decreases for masses which correspond to scales at which there is decrement in power. This also means that collapse fraction falls as  $z_f(m_a)$  decreases.

It is not straightforward to compare the theoretical collapsed fraction (Eq. (5.1)) with the damped Lyman- $\alpha$  data because there is a large uncertainty in the masses of these clouds. Simulations suggest that the mass of damped- $\alpha$  clouds could lie in the range  $10^9$ – $10^{10} M_\odot$  ([94]). However, recent observations suggest that the mass could be as high as  $10^{12} M_\odot$  at  $z \simeq 2.5$ . ([95]). For the present work, we assume two halo masses  $10^{10}$  and  $5 \times 10^{10} M_\odot$  as the threshold masses for the formation of Damped Lyman- $\alpha$  clouds. We compute the collapsed fraction for comparison with the data by integrating the mass function with threshold mass as lower limits.

In Figures 9 and 10 we compare the prediction of LFDm and ULA models with the damped Lyman- $\alpha$  data. As noted above, the damped Lyman- $\alpha$  data provide a lower limit to the collapsed fraction. Therefore, all models that predict collapsed fraction smaller than the data can be ruled out. As expected, the constraints are tighter for the higher threshold halo mass. Figures 9 and 10 show that  $z_f < 2 \times 10^5$  and  $m_a < 10^{-23}$  eV can be ruled out from the present data. It should be noted that the data at higher redshifts provide tighter bounds.

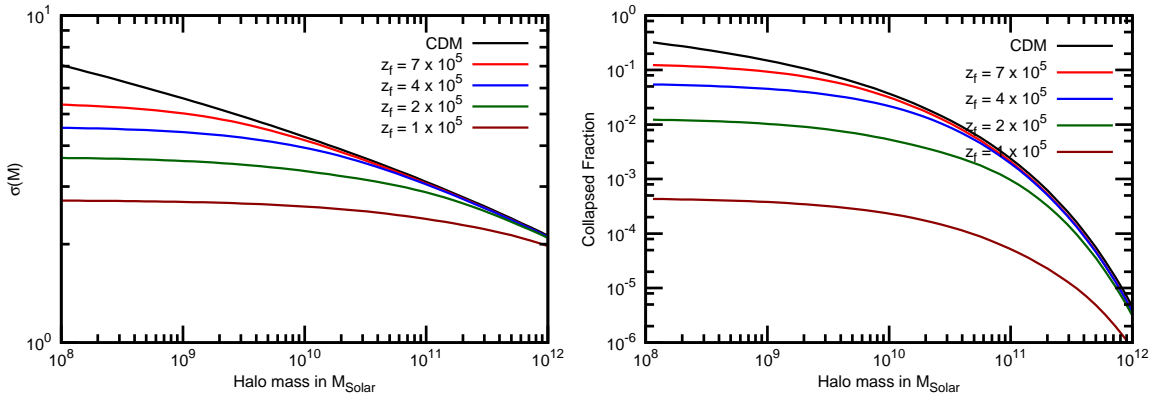


**Figure 7.** The mass dispersion  $\sigma_M$  is shown for a range of LFDm models (Left Panel). The right panel shows the collapse fraction as a function of halo mass. Both the panels are for  $z = 6$ .

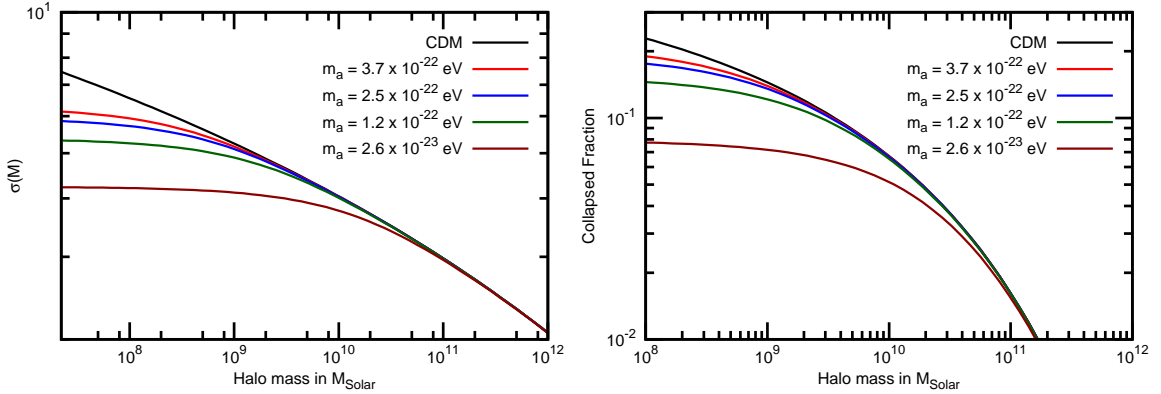


**Figure 8.** The same as Figure 7 for ULA models.

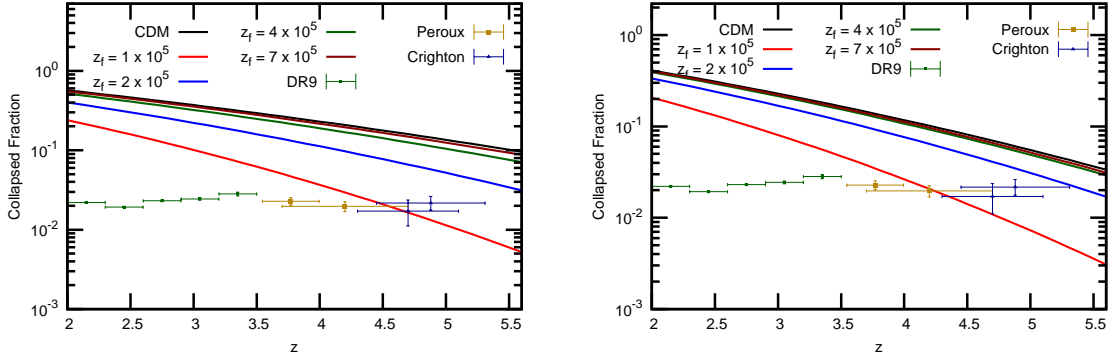


**Figure 9.** The redshift evolution of collapsed fraction for LFDM models is shown along with with the data from Damped Lyman- $\alpha$  absorption data [54, 56, 57]. The left (right) panels correspond to threshold halo masses  $M = 10^{10} M_{\odot}$  ( $M = 5 \times 10^{10} M_{\odot}$ ), respectively.

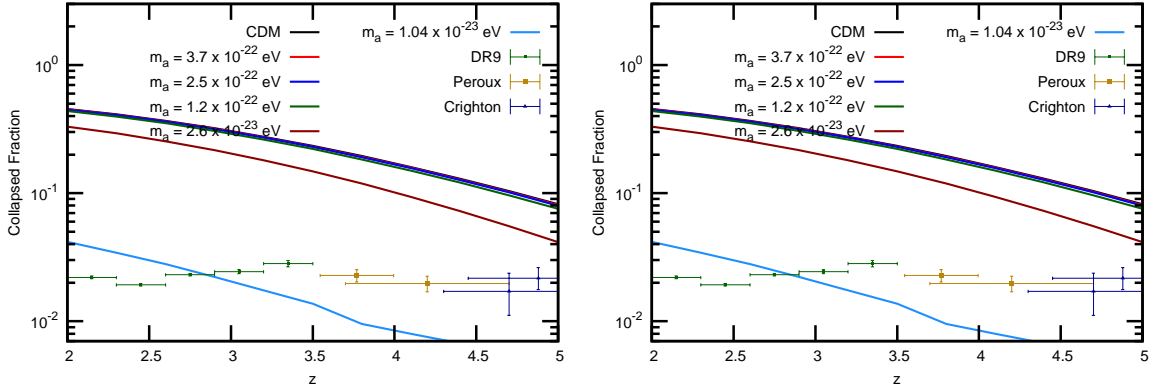


**Figure 10.** The same as Figure 9 for ULA models

## 6 Conclusion

From cosmological observations we know that DM must display clustering properties similar to CDM, at least on the largest scales. However, the particle nature of DM is still not known. The linear LSS observations, such as WiggleZ, BOSS, and Planck data on CMB temperature and polarization anisotropies can be used to place very stringent constraints on any dark matter models that show deviation from the  $\Lambda$ CDM model for  $k < 0.1 \text{ Mpc}^{-1}$  [1, 51, 63]. However, at smaller scales the situation remains unclear from astrophysical observables, e.g. the missing satellite problem [29, 30]. This points to a need to study plausible dark matter models that allow for significant deviation from  $\Lambda$ CDM models at small scales and confront them with astrophysical and cosmological observables. This paper is one step in that direction.

In this paper, we consider the implications, and possible constraints on, of a class of LFDM and axion-inspired models by running a series of N-body and reionization field numerical simulations with the appropriate power spectra as initial conditions. Specifically, we study the reionization epoch and the evolution of the collapsed fraction of matter at high redshifts. Such models generically give a decrement in matter power at small scales. In particular, we study the HI signal from the epoch of reionization. We also consider the evolution of the collapsed fraction of the matter in the redshift range  $2 < z < 5$ , using the data of damped Lyman- $\alpha$  on  $\Omega_{\text{HI}}(z)$ .

We show that the power spectrum of the HI field could be higher for such models for a fixed ionization fraction as compared to the  $\Lambda$ CDM model. The enhancement is by factors of 2–10 for range of scales  $0.1 < k < 4 \text{ Mpc}^{-1}$ . (Figure 6).

For studying the EoR with alternative DM models, we demand that these models be able to provide a reionization fraction  $x = 0.5$  at  $z = 8$ . For very low  $z_f$  and  $m_a$ , no halos are formed at  $z = 8$  in the N-body box, which rules out of these models. In models with larger  $z_f$  and  $m_a$ , the desired amount of reionization is achieved by increasing the number of ionizing photons,  $N_{\text{ion}}$  as compared to the  $\Lambda$ CDM model. The models that require unrealistically large value of the number of ionizing photons are also excluded. These considerations are listed in Table 1 and lead to generic bounds on the epoch of the formation of dark matter  $z_f > 4 \times 10^5$  and the axion mass  $m_a > 2.6 \times 10^{-23} \text{ eV}$ . We also obtain weaker constraints from the damped Lyman- $\alpha$  data on the evolution of collapsed gas fraction:  $z_f > 2 \times 10^5$  and  $m_a > 10^{-23} \text{ eV}$ .

The models we consider in this paper have been studied in the context of other cosmological observables. The LFDm models have been compared against the SDSS galaxy clustering and the Lyman- $\alpha$  data [60]; the SDSS data gives  $z_f > 10^5$  while the Lyman- $\alpha$  data results in stronger bounds  $z_f > 9 \times 10^5$  (all  $3\sigma$ ). While the Lyman- $\alpha$  data give more stringent constraints than we obtain here, the models consistent with this data still result in an enhancement of up to a factor of 4 in the HI power spectra (Figure 6). The ULA models considered here have been confronted with Lyman- $\alpha$  and galaxy luminosity data; the resulting bounds are  $m_a > 10^{-22} \text{ eV}$  which are comparable to the constraints we obtain this paper [65, 76]. It is interesting to note that the current constraints on ULAs, including our own, are consistent with the mass necessary for a successful solution of the cusp-core problem in dwarf spheroidals [27, 48, 49, 96].

Building a physical model of the nature of dark matter consistent with all the astrophysical and cosmological observables has not been achieved yet. Cosmological observables affected by small scale matter power remain crucial elements in this quest. In this paper we studied the impact of two such observables for two classes of non-WIMP dark matter models and were able to constrain their underlying parameters. In the future we hope to return to this issue with further comparisons with the low and high redshift astrophysical data.

## Acknowledgements

DJEM acknowledges the support of a Royal Astronomical Society post-doctoral research fellowship, hosted at King's College London. DJEM also acknowledges useful discussions with Hsi-Yu Schive.

## References

- [1] **Planck** Collaboration, P. Ade et al., *Planck 2013 results. XVI. Cosmological parameters*, *Astron.Astrophys.* (2014) [[arXiv:1303.5076](#)].
- [2] **WMAP** Collaboration, G. Hinshaw et al., *Nine-Year Wilkinson Microwave Anisotropy Probe (WMAP) Observations: Cosmological Parameter Results*, *Astrophys.J.Suppl.* **208** (2013) 19, [[arXiv:1212.5226](#)].
- [3] **Atacama Cosmology Telescope** Collaboration, J. L. Sievers et al., *The Atacama Cosmology Telescope: Cosmological parameters from three seasons of data*, *JCAP* **1310** (2013) 060, [[arXiv:1301.0824](#)].
- [4] **SDSS** Collaboration, M. Tegmark et al., *Cosmological Constraints from the SDSS Luminous Red Galaxies*, *Phys.Rev.* **D74** (2006) 123507, [[astro-ph/0608632](#)].
- [5] **SDSS** Collaboration, M. Tegmark et al., *Cosmological parameters from SDSS and WMAP*, *Phys.Rev.* **D69** (2004) 103501, [[astro-ph/0310723](#)].
- [6] K. Begeman, A. Broeils, and R. Sanders, *Extended rotation curves of spiral galaxies: Dark haloes and modified dynamics*, *Mon.Not.Roy.Astron.Soc.* **249** (1991) 523.
- [7] M. Bartelmann and P. Schneider, *Weak gravitational lensing*, *Phys.Rept.* **340** (2001) 291–472, [[astro-ph/9912508](#)].
- [8] G. Angloher, M. Bauer, I. Bavykina, A. Bento, C. Bucci, et al., *Results from 730 kg days of the CRESST-II Dark Matter Search*, *Eur.Phys.J.* **C72** (2012) 1971, [[arXiv:1109.0702](#)].
- [9] **XENON100 Collaboration** Collaboration, E. Aprile et al., *First Dark Matter Results from the XENON100 Experiment*, *Phys.Rev.Lett.* **105** (2010) 131302, [[arXiv:1005.0380](#)].

- [10] **XENON100 Collaboration** Collaboration, E. Aprile et al., *Dark Matter Results from 225 Live Days of XENON100 Data*, Phys.Rev.Lett. **109** (2012) 181301, [[arXiv:1207.5988](#)].
- [11] **CDMS-II Collaboration** Collaboration, Z. Ahmed et al., *Results from a Low-Energy Analysis of the CDMS II Germanium Data*, Phys.Rev.Lett. **106** (2011) 131302, [[arXiv:1011.2482](#)].
- [12] **LUX Collaboration** Collaboration, D. Akerib et al., *First results from the LUX dark matter experiment at the Sanford Underground Research Facility*, Phys.Rev.Lett. **112** (2014) 091303, [[arXiv:1310.8214](#)].
- [13] **PAMELA Collaboration** Collaboration, O. Adriani et al., *An anomalous positron abundance in cosmic rays with energies 1.5-100 GeV*, Nature **458** (2009) 607–609, [[arXiv:0810.4995](#)].
- [14] **PAMELA Collaboration** Collaboration, O. Adriani et al., *PAMELA results on the cosmic-ray antiproton flux from 60 MeV to 180 GeV in kinetic energy*, Phys.Rev.Lett. **105** (2010) 121101, [[arXiv:1007.0821](#)].
- [15] O. Adriani, G. Barbarino, G. Bazilevskaya, R. Bellotti, M. Boezio, et al., *A new measurement of the antiproton-to-proton flux ratio up to 100 GeV in the cosmic radiation*, Phys.Rev.Lett. **102** (2009) 051101, [[arXiv:0810.4994](#)].
- [16] **PAMELA Collaboration** Collaboration, O. Adriani et al., *The cosmic-ray electron flux measured by the PAMELA experiment between 1 and 625 GeV*, Phys.Rev.Lett. **106** (2011) 201101, [[arXiv:1103.2880](#)].
- [17] **Fermi LAT Collaboration** Collaboration, M. Ackermann et al., *Measurement of separate cosmic-ray electron and positron spectra with the Fermi Large Area Telescope*, Phys.Rev.Lett. **108** (2012) 011103, [[arXiv:1109.0521](#)].
- [18] **Fermi LAT Collaboration** Collaboration, M. Ackermann et al., *Fermi LAT observations of cosmic-ray electrons from 7 GeV to 1 TeV*, Phys.Rev. **D82** (2010) 092004, [[arXiv:1008.3999](#)].
- [19] **Fermi LAT Collaboration** Collaboration, A. A. Abdo et al., *Measurement of the Cosmic Ray  $e^+$  plus  $e^-$  spectrum from 20 GeV to 1 TeV with the Fermi Large Area Telescope*, Phys.Rev.Lett. **102** (2009) 181101, [[arXiv:0905.0025](#)].
- [20] **HEAT Collaboration** Collaboration, S. Barwick et al., *Measurements of the cosmic ray positron fraction from 1-GeV to 50-GeV*, Astrophys.J. **482** (1997) L191–L194, [[astro-ph/9703192](#)].
- [21] **AMS-01 Collaboration** Collaboration, M. Aguilar et al., *Cosmic-ray positron fraction measurement from 1 to 30-GeV with AMS-01*, Phys.Lett. **B646** (2007) 145–154, [[astro-ph/0703154](#)].
- [22] J. Goodman, M. Ibe, A. Rajaraman, W. Shepherd, T. M. Tait, et al., *Constraints on Light Majorana dark Matter from Colliders*, Phys.Lett. **B695** (2011) 185–188, [[arXiv:1005.1286](#)].
- [23] P. J. Fox, R. Harnik, J. Kopp, and Y. Tsai, *Missing Energy Signatures of Dark Matter at the LHC*, Phys.Rev. **D85** (2012) 056011, [[arXiv:1109.4398](#)].
- [24] D. Hooper, *Revisiting XENON100's Constraints (and Signals?) For Low-Mass Dark Matter*, JCAP **1309** (2013) 035, [[arXiv:1306.1790](#)].
- [25] W. J. G. de Blok, *The Core-Cusp Problem*, Adv. Astron. **2010** (2010) 789293, [[arXiv:0910.3538](#)].
- [26] J. F. Navarro, C. S. Frenk, and S. D. M. White, *The Structure of cold dark matter halos*, Astrophys. J. **462** (1996) 563–575, [[astro-ph/9508025](#)].
- [27] M. G. Walker and J. Penarrubia, *A Method for Measuring (Slopes of) the Mass Profiles of Dwarf Spheroidal Galaxies*, Astrophys. J. **742** (2011) 20, [[arXiv:1108.2404](#)].
- [28] T. Richardson and M. Fairbairn, *On the dark matter profile in sculptor: breaking the  $\beta$  degeneracy with virial shape parameters*, Monthly Notices of the Royal Astronomical Society **441** (2014), no. 2 1584–1600, [<http://mnr.as.oxfordjournals.org/content/441/2/1584.full.pdf+html>].
- [29] A. A. Klypin, A. V. Kravtsov, O. Valenzuela, and F. Prada, *Where are the missing Galactic satellites?*, Astrophys.J. **522** (1999) 82–92, [[astro-ph/9901240](#)].
- [30] B. Moore, S. Ghigna, F. Governato, G. Lake, T. R. Quinn, et al., *Dark matter substructure within galactic halos*, Astrophys.J. **524** (1999) L19–L22, [[astro-ph/9907411](#)].
- [31] S. Garrison-Kimmel, M. Boylan-Kolchin, J. S. Bullock, and E. N. Kirby, *Too Big to Fail in the Local Group*, [[arXiv:1404.5313](#)].
- [32] M. Boylan-Kolchin, J. S. Bullock, and M. Kaplinghat, *Too big to fail? The puzzling darkness of massive Milky Way subhaloes*, Mon.Not.Roy.Astron.Soc. **415** (2011) L40, [[arXiv:1103.0007](#)].

- [33] M. S. Pawlowski, B. Famaey, D. Merritt, and P. Kroupa, *On the persistence of two small-scale problems in  $\Lambda$ CDM*, [arXiv:1510.08060](#).
- [34] J. Oñorbe, M. Boylan-Kolchin, J. S. Bullock, P. F. Hopkins, D. Kereš, C.-A. Faucher-Giguère, E. Quataert, and N. Murray, *Forged in FIRE: cusps, cores and baryons in low-mass dwarf galaxies*, Mon. Not. Roy. Astron. Soc. **454** (Dec., 2015) 2092–2106, [[arXiv:1502.02036](#)].
- [35] T. Sawala, C. S. Frenk, A. Fattahi, J. F. Navarro, R. G. Bower, R. A. Crain, C. Dalla Vecchia, M. Furlong, J. C. Helly, A. Jenkins, K. A. Oman, M. Schaller, J. Schaye, T. Theuns, J. Trayford, and S. D. M. White, *Local Group galaxies emerge from the dark*, [ArXiv e-prints](#) (Dec., 2014) [[arXiv:1412.2748](#)].
- [36] A. Dolgov and S. Hansen, *Massive sterile neutrinos as warm dark matter*, Astropart.Phys. **16** (2002) 339–344, [[hep-ph/0009083](#)].
- [37] M. Viel, J. Lesgourgues, M. G. Haehnelt, S. Matarrese, and A. Riotto, *Constraining warm dark matter candidates including sterile neutrinos and light gravitinos with WMAP and the Lyman-alpha forest*, Phys.Rev. **D71** (2005) 063534, [[astro-ph/0501562](#)].
- [38] P. Bode, J. P. Ostriker, and N. Turok, *Halo formation in warm dark matter models*, The Astrophysical Journal **556** (2001), no. 1 93.
- [39] E. Polisensky and M. Ricotti, *Constraints on the Dark Matter Particle Mass from the Number of Milky Way Satellites*, Phys. Rev. **D83** (2011) 043506, [[arXiv:1004.1459](#)].
- [40] D. Anderhalden, J. Diemand, G. Bertone, A. V. Maccio, and A. Schneider, *The Galactic Halo in Mixed Dark Matter Cosmologies*, JCAP **1210** (2012) 047, [[arXiv:1206.3788](#)].
- [41] M. R. Lovell, V. Eke, C. S. Frenk, L. Gao, A. Jenkins, T. Theuns, J. Wang, D. M. White, A. Boyarsky, and O. Ruchayskiy, *The Haloes of Bright Satellite Galaxies in a Warm Dark Matter Universe*, Mon. Not. Roy. Astron. Soc. **420** (2012) 2318–2324, [[arXiv:1104.2929](#)].
- [42] A. V. Maccio, S. Paduroiu, D. Anderhalden, A. Schneider, and B. Moore, *Cores in warm dark matter haloes: a Catch 22 problem*, Mon. Not. Roy. Astron. Soc. **424** (2012) 1105–1112, [[arXiv:1202.1282](#)].
- [43] A. Schneider, R. E. Smith, A. V. Maccio, and B. Moore, *Nonlinear Evolution of Cosmological Structures in Warm Dark Matter Models*, Mon. Not. Roy. Astron. Soc. **424** (2012) 684, [[arXiv:1112.0330](#)].
- [44] J. Baur, N. Palanque-Delabrouille, C. Yèche, C. Magneville, and M. Viel, *Lyman-alpha Forests cool Warm Dark Matter*, 2015. [arXiv:1512.01981](#).
- [45] S. Das and N. Weiner, *Late Forming Dark Matter in Theories of Neutrino Dark Energy*, Phys.Rev. **D84** (2011) 123511, [[astro-ph/0611353](#)].
- [46] A. Arvanitaki, S. Dimopoulos, S. Dubovsky, N. Kaloper, and J. March-Russell, *String Axiverse*, Phys. Rev. **D81** (2010) 123530, [[arXiv:0905.4720](#)].
- [47] S. Agarwal, P. S. Corasaniti, S. Das, and Y. Rasera, *Small scale clustering of late forming dark matter*, [arXiv:1412.1103](#).
- [48] H.-Y. Schive, T. Chiueh, and T. Broadhurst, *Cosmic Structure as the Quantum Interference of a Coherent Dark Wave*, Nature Phys. **10** (2014) 496–499, [[arXiv:1406.6586](#)].
- [49] D. J. E. Marsh and A.-R. Pop, *Axion dark matter, solitons and the cusp-core problem*, Mon. Not. Roy. Astron. Soc. **451** (2015), no. 3 2479–2492, [[arXiv:1502.03456](#)].
- [50] D. J. E. Marsh, *Axion Cosmology*, [arXiv:1510.07633](#).
- [51] **Planck** Collaboration, P. A. R. Ade et al., *Planck 2015 results. XIII. Cosmological parameters*, [arXiv:1502.01589](#).
- [52] **SDSS** Collaboration, X. Fan et al., *The Discovery of a luminous  $z = 5.80$  quasar from the Sloan Digital Sky Survey*, Astron. J. **120** (2000) 1167–1174, [[astro-ph/0005414](#)].
- [53] R. Barkana and A. Loeb, *In the beginning: The First sources of light and the reionization of the Universe*, Phys. Rept. **349** (2001) 125–238, [[astro-ph/0010468](#)].
- [54] P. Noterdaeme, P. Petitjean, C. Ledoux, and R. Srianand, *Evolution of the cosmological mass density of neutral gas from Sloan Digital Sky Survey II - Data Release 7*, Astron. Astrophys. **505** (2009) 1087, [[arXiv:0908.1574](#)].

- [55] C. Peroux, R. G. McMahon, L. J. Storrie-Lombardi, and M. J. Irwin, *The evolution of  $\omega(\text{HI})$  and the epoch of formation of damped Lyman-alpha absorbers*, Mon. Not. Roy. Astron. Soc. **346** (2003) 1103, [[astro-ph/0107045](#)].
- [56] P. Noterdaeme et al., *Column density distribution and cosmological mass density of neutral gas: Sloan Digital Sky Survey-III Data Release 9*, Astron. Astrophys. **547** (2012) L1, [[arXiv:1210.1213](#)].
- [57] T. Zafar, C. Peroux, A. Popping, B. Milliard, J.-M. Deharveng, and S. Frank, *The ESO UVES Advanced Data Products Quasar Sample - II. Cosmological Evolution of the Neutral Gas Mass Density*, Astron. Astrophys. **556** (2013) A141, [[arXiv:1307.0602](#)].
- [58] S. Bharadwaj and P. S. Srikant, *HI fluctuations at large redshifts. 3. Simulating the signal expected at GMRT*, J. Astrophys. Astron. **25** (2004) 67, [[astro-ph/0402262](#)].
- [59] R. Mondal, S. Bharadwaj, S. Majumdar, A. Bera, and A. Acharyya, *The effect of non-Gaussianity on error predictions for the Epoch of Reionization (EoR) 21-cm power spectrum*, Mon. Not. Roy. Astron. Soc. **449** (2015), no. 1 L41–L45, [[arXiv:1409.4420](#)].
- [60] A. Sarkar, S. Das, and S. K. Sethi, *How Late can the Dark Matter form in our universe?*, JCAP **1503** (2015), no. 03 004, [[arXiv:1410.7129](#)].
- [61] S. Das, *Sterile neutrino, hidden dark matter and their cosmological signatures*, J. Phys. Conf. Ser. **405** (2012) 012011.
- [62] W. Hu, R. Barkana, and A. Gruzinov, *Cold and fuzzy dark matter*, Phys. Rev. Lett. **85** (2000) 1158–1161, [[astro-ph/0003365](#)].
- [63] R. Hlozek, D. Grin, D. J. E. Marsh, and P. G. Ferreira, *A search for ultralight axions using precision cosmological data*, Phys. Rev. D **91** (May, 2015) 103512.
- [64] B. Bozek, D. J. E. Marsh, J. Silk, and R. F. G. Wyse, *Galaxy UV-luminosity function and reionization constraints on axion dark matter*, Mon. Not. Roy. Astron. Soc. **450** (2015), no. 1 209–222, [[arXiv:1409.3544](#)].
- [65] L. Amendola and R. Barbieri, *Dark matter from an ultra-light pseudo-Goldstone-boson*, Phys. Lett. **B642** (2006) 192–196, [[hep-ph/0509257](#)].
- [66] D. J. E. Marsh and P. G. Ferreira, *Ultra-Light Scalar Fields and the Growth of Structure in the Universe*, Phys. Rev. **D82** (2010) 103528, [[arXiv:1009.3501](#)].
- [67] D. J. E. Marsh, E. Macaulay, M. Trebitsch, and P. G. Ferreira, *Ultra-light Axions: Degeneracies with Massive Neutrinos and Forecasts for Future Cosmological Observations*, Phys. Rev. **D85** (2012) 103514, [[arXiv:1110.0502](#)].
- [68] D. J. E. Marsh and J. Silk, *A Model For Halo Formation With Axion Mixed Dark Matter*, Mon. Not. Roy. Astron. Soc. **437** (2014), no. 3 2652–2663, [[arXiv:1307.1705](#)].
- [69] L. A. Ureña-López and A. X. Gonzalez-Morales, *Towards accurate cosmological predictions for rapidly oscillating scalar fields as dark matter*, [[arXiv:1511.08195](#)].
- [70] C.-G. Park, J.-c. Hwang, and H. Noh, *Axion as a cold dark matter candidate: low-mass case*, Phys. Rev. **D86** (2012) 083535, [[arXiv:1207.3124](#)].
- [71] M. Kuhlen and C. A. Faucher-Giguere, *Concordance models of reionization: implications for faint galaxies and escape fraction evolution*, Mon. Not. Roy. Astron. Soc. **423** (2012) 862–876, [[arXiv:1201.0757](#)].
- [72] S. Furlanetto, M. Zaldarriaga, and L. Hernquist, *The Growth of HII regions during reionization*, Astrophys. J. **613** (2004) 1–15, [[astro-ph/0403697](#)].
- [73] R. Mondal, S. Bharadwaj, and S. Majumdar, *Statistics of the epoch of reionization (EoR) 21-cm signal: I - power spectrum error covariance*, [[arXiv:1508.00896](#)].
- [74] A. Mesinger and S. Furlanetto, *Efficient Simulations of Early Structure Formation and Reionization*, Astrophys. J. **669** (2007) 663, [[arXiv:0704.0946](#)].
- [75] R. K. Sheth and G. Tormen, *An Excursion set model of hierarchical clustering : Ellipsoidal collapse and the moving barrier*, Mon. Not. Roy. Astron. Soc. **329** (2002) 61, [[astro-ph/0105113](#)].
- [76] H.-Y. Schive, T. Chiueh, T. Broadhurst, and K.-W. Huang, *Contrasting Galaxy Formation from Quantum Wave Dark Matter,  $\psi\text{DM}$ , with  $\Lambda\text{CDM}$ , using Planck and Hubble Data*, [[arXiv:1508.04621](#)].

- [77] J. Wang and S. D. M. White, *Discreteness effects in simulations of Hot/Warm dark matter*, Mon. Not. Roy. Astron. Soc. **380** (2007) 93–103, [[astro-ph/0702575](#)].
- [78] M. R. Lovell, C. S. Frenk, V. R. Eke, A. Jenkins, L. Gao, and T. Theuns, *The properties of warm dark matter haloes*, Mon. Not. Roy. Astron. Soc. **439** (2014) 300–317, [[arXiv:1308.1399](#)].
- [79] A. Schneider, R. E. Smith, and D. Reed, *Halo Mass Function and the Free Streaming Scale*, Mon. Not. Roy. Astron. Soc. **433** (2013) 1573, [[arXiv:1303.0839](#)].
- [80] P. Mocz and S. Succi, *Numerical solution of the nonlinear Schrodinger equation using smoothed-particle hydrodynamics*, Phys. Rev. **E91** (2015), no. 5 053304, [[arXiv:1503.03869](#)].
- [81] S. Agarwal and P. S. Corasaniti, *Structural properties of artificial halos in nonstandard dark matter simulations*, Phys. Rev. **D91** (2015), no. 12 123509, [[arXiv:1503.03503](#)].
- [82] T. R. Choudhury, M. G. Haehnelt, and J. Regan, *Inside-out or Outside-in: The topology of reionization in the photon-starved regime suggested by Lyman-alpha forest data*, Mon. Not. Roy. Astron. Soc. **394** (2009) 960, [[arXiv:0806.1524](#)].
- [83] S. Bharadwaj and S. S. Ali, *The CMBR fluctuations from HI perturbations prior to reionization*, Mon. Not. Roy. Astron. Soc. **352** (2004) 142, [[astro-ph/0401206](#)].
- [84] S. Majumdar, S. Bharadwaj, and T. R. Choudhury, *The effect of peculiar velocities on the epoch of reionization (EoR) 21-cm signal*, Mon. Not. Roy. Astron. Soc. **434** (2012), no. 3 1978–1988, [[arXiv:1209.4762](#)].
- [85] S. Bharadwaj and S. S. Ali, *On using visibility correlations to probe the HI distribution from the dark ages to the present epoch. I. Formalism and the expected signal*, Mon. Not. Roy. Astron. Soc. **356** (2005) 1519, [[astro-ph/0406676](#)].
- [86] R. Salvaterra and A. Ferrara, *Where are the sources of the near infrared background?*, Mon. Not. Roy. Astron. Soc. **367** (2006) L11–L15, [[astro-ph/0509338](#)].
- [87] B. Yue, A. Ferrara, R. Salvaterra, and X. Chen, *The Contribution of High Redshift Galaxies to the Near-Infrared Background*, Mon. Not. Roy. Astron. Soc. **431** (2013) 383, [[arXiv:1208.6234](#)].
- [88] N. Kaiser, *On the Spatial correlations of Abell clusters*, Astrophys. J. **284** (1984) L9–L12.
- [89] P. J. E. Peebles, Principles of Physical Cosmology. Princeton University Press, 1993.
- [90] A. Lidz, O. Zahn, M. McQuinn, M. Zaldarriaga, and L. Hernquist, *Detecting the Rise and Fall of 21 cm Fluctuations with the Murchison Widefield Array*, Astrophys. J. **680** (2008) 962–974, [[arXiv:0711.4373](#)].
- [91] S. K. Sethi and K. Subramanian, *Primordial magnetic fields and the HI signal from the epoch of reionization*, JCAP **0911** (2009) 021, [[arXiv:0911.0244](#)].
- [92] J. C. Pober et al., *PAPER-64 Constraints on Reionization II: The Temperature of the  $z = 8.4$  Intergalactic Medium*, Astrophys. J. **809** (2015), no. 1 62, [[arXiv:1503.00045](#)].
- [93] R. K. Sheth and G. Tormen, *Large scale bias and the peak background split*, Mon. Not. Roy. Astron. Soc. **308** (1999) 119, [[astro-ph/9901122](#)].
- [94] A. Pontzen, F. Governato, M. Pettini, C. M. Booth, G. Stinson, J. Wadsley, A. Brooks, T. R. Quinn, and M. Haehnelt, *Damped Lyman Alpha Systems in Galaxy Formation Simulations*, Mon. Not. Roy. Astron. Soc. **390** (2008) 1349, [[arXiv:0804.4474](#)].
- [95] A. Font-Ribera et al., *The large-scale cross-correlation of Damped Lyman Alpha Systems with the Lyman Alpha Forest: First Measurements from BOSS*, JCAP **1211** (2012) 059, [[arXiv:1209.4596](#)].
- [96] H.-Y. Schive, M.-H. Liao, T.-P. Woo, S.-K. Wong, T. Chiueh, T. Broadhurst, and W. Y. P. Hwang, *Understanding the Core-Halo Relation of Quantum Wave Dark Matter from 3D Simulations*, Phys. Rev. Lett. **113** (2014), no. 26 261302, [[arXiv:1407.7762](#)].